ADAPTIVE, CONSERVATIVE SOLUTION OF THE FOKKER-PLANCK EQUATION IN MOLECULAR BIOLOGY

LARS FERM[1], PER LÖTSTEDT[1], PAUL SJÖBERG[1] *

[1] *Div of Scientific Computing, Dept of Information Technology*
Uppsala University, SE-75105 Uppsala, Sweden
emails: ferm, perl, pauls @it.uu.se

Abstract

The Fokker-Planck equation on conservation form is discretized by a finite volume method and advanced in time by a linear multistep method. The grid cells are refined and coarsened in blocks of the grid depending on an estimate of the spatial discretization error and the time step is chosen to satisfy a tolerance on the temporal discretization error. The solution is conserved across the block boundaries so that the total probability is constant. A similar effect is achieved by rescaling the solution. The steady state solution is determined as the eigenvector corresponding to the zero eigenvalue. The method is applied to the solution of a problem with two molecular species and the simulation of a circadian clock. Comparison is made with a stochastic method.

Keywords: Fokker-Planck equation, finite volume method, adaptive method, probability density, conservation

AMS subject classification: 65M20, 65M50

1 Introduction

The spectacular progress of molecular biology during the last decade has given us more or less complete maps of the genome of several species and methods for quantitative experiments on single cells. The large amount of data has made it obvious that there is a demand for new techniques for understanding the sum of the parts. The branch of molecular biology that has accepted this challenge is

*Financial support has been obtained from the Swedish Foundation for Strategic Research and the Swedish National Graduate School in Scientific Comptuing.

sometimes called systems biology [5]. An important tool of systems biology is to use simple models for computer investigation of the principles of regulation of gene expression and biochemical pathways.

The standard model for chemical reactions in molecular biology is the reaction rate equations. They are a system of nonlinear ordinary differential equations (ODEs) for the concentrations of the molecular species in the reactions. This model is deterministic and suitable for reactions with many participating molecules of each species. If the number of molecules is small or if the reactions occur far from thermodynamic equilibrium, then a stochastic model such as the master equation [6, 7, 13, 19] is much more accurate. The master equation is a differential-difference equation for the time dependent probability density p of the number of molecules of each species. With N different species, the spatial domain of p is an N-dimensional space.

The Fokker-Planck (FP) equation is a partial differential equation (PDE) in time and N-dimensional space approximating the master equation. For small N, the FP equation can be solved numerically after discretization, but for $N \gtrsim 5$ other methods are needed due to the exponential growth of computational work and storage requirements with increasing N ('the curse of dimensionality'). A deterministic method for high dimensions is to use sparse grids [3]. A stochastic method is Gillespie's algorithm [10], which is a Monte Carlo method simulating the reactions step by step. This is the usual method in molecular biology to compute the time evolution of the probability distribution of chemical compositions also for small N. We show in this paper that numerical solution of the FP equation is an alternative for low dimensions with many advantages and illustrate our method with two two-dimensional examples.

The FP equation is discretized in the nonnegative orthant by a finite volume method. The boundary conditions are such that the total probability density is constant over time. The grid is Cartesian and is adaptively refined and coarsened in blocks of the grid [8]. A pioneering Adaptive Mesh Refinement (AMR) algorithm is found in [2] and in [14] the efficiency of grid adaptation is evaluated experimentally. Estimates of the spatial discretization error determine where finer or coarser cells are introduced. At a block boundary, the cell size is allowed to increase by a factor two. The time integration is implicit and in each time step a system of linear equations is solved iteratively for p. The time step is chosen so that the estimated temporal discretization error is below some given threshold [16]. Second order accuracy is obtained also at block boundaries. The scheme is conservative after corrections at the block boundaries but then formal accuracy is reduced to one there. The total probability is preserved with a conservative discretization. The same effect is achieved by rescaling the solution now and then.

The steady state solution of the FP equation is computed with adaptation by solving an eigenvalue problem for a few eigenvalues with Arnoldi's method [15]. The solution is the eigenvector corresponding to the zero eigenvalue. The

operator of the conservative scheme is guaranteed to have a zero eigenvalue. This may not be the case for the non-conservative method. This way of computing the steady state solution is orders of magnitude faster than integrating the time dependent solution until the time derivatives vanish.

The method is first applied to a system with two species modeling two reacting metabolites created by two enzymes in a growing cell [7]. Then the FP equation corresponding to the model of the circadian clock in [20] is solved. The circadian clock is a biological rhythm responsible for adapting organisms to periodic variations in their terrestial environment such as the daylight [11]. This equation is sensitive to the formulation of the boundary conditions. The FP solution is compared to the solution obtained by Gillespie's method.

The supremum norm for a vector v of length N is denoted by $|v|_\infty$ and the ℓ_2-norm is $\|v\|_2 = (\sum_{i=1}^N |v_i|^2)^{1/2}$ in the paper.

2 The master and Fokker-Planck equations

The chemical reactions in a cell can be modelled by macroscopic, deterministic equations or by mesoscopic, stochastic equations. The concentrations of the chemical species satisfy a system of ODEs on a macroscale. The probability density for the participating molecules satisfies a master equation on a mesoscale. These equations are discussed in this section and the solution of the master equation is approximated by the solution of the FP equation. The assumption is that the mixture of molecules is spatially homogeneous so that space dependent solutions are avoided.

Assume that we have N chemically active molecular species $X_i,\ i = 1 \dots N$, and that there are x_i molecules of substrate X_i at time t. The state vector $\mathbf{x}$ of dimension N satisfies $\mathbf{x} \in \mathbb{Z}_+^N$, where $\mathbb{Z}_+$ denotes the non-negative integer numbers. The inequality relation $\mathbf{x} \geq 0$ for a vector $\mathbf{x}$ denotes that all components are non-negative $x_i \geq 0,\ i = 1 \dots N$. A chemical reaction r is a transition from a state $\mathbf{x}_r$ to $\mathbf{x}$ so that $\mathbf{x}_r = \mathbf{x} + \mathbf{n}_r$. The probability or propensity for the reaction to occur per unit time is $w_r(\mathbf{x}_r) \in \mathbb{R}$. The propensity is non-negative and often modeled as a polynomial or a rational polynomial in x_i. The reaction r can be written

$$\mathbf{x}_r \xrightarrow{w_r(\mathbf{x}_r)} \mathbf{x},\ \mathbf{n}_r = \mathbf{x}_r - \mathbf{x}. \tag{1}$$

The time evolution of the concentrations of the molecules is governed by the reaction rate equations. They form a system of N coupled nonlinear ODEs, which are valid when the molecular copy number of each species is large. Let the concentration of X_i be denoted by $[x_i]$ and let $[\mathbf{x}] \in \mathbb{R}_+^N$ be the vector of concentrations, where $\mathbb{R}_+$ denotes the non-negative real numbers. Then the reaction

rate equations with R reactions are [13]

$$\frac{d[x_i]}{dt} = -\sum_{r=1}^{R} \mathbf{n}_{ri} w_r([\mathbf{x}]),\ i = 1 \dots N. \tag{2}$$

The system (2) is often stiff with the size of the terms in w_r differing by orders of magnitude.

The master equation is a difference-differential equation for the time evolution of the probability density $p(\mathbf{x}, t)$ that the molecular state is $\mathbf{x}$ at time t [13]. To derive the equation for p, split $\mathbf{n}_r$ into two parts so that

$$\mathbf{n}_r = \mathbf{n}_r^+ + \mathbf{n}_r^-, n_{ri}^+ = \max(n_{ri}, 0), n_{ri}^- = \min(n_{ri}, 0).$$

A reaction (1) at $\mathbf{x}_r$ takes place if $\mathbf{x}_r \geq 0$ and $\mathbf{x} \geq 0$ implying that $\mathbf{x} + \mathbf{n}_r^- \geq 0$, and a reaction at $\mathbf{x}$ occurs if $\mathbf{x} \geq 0$ and $\mathbf{x} - \mathbf{n}_r \geq 0$ implying that $\mathbf{x} - \mathbf{n}_r^+ \geq 0$. Introduce the flux for the r:th reaction

$$q_r(\mathbf{x}, t) = w_r(\mathbf{x}, t) p(\mathbf{x}, t).$$

For a single reaction the change of probability is

$$\frac{\partial p(\mathbf{x}, t)}{\partial t} = \left\{ \begin{array}{cc} q_r(\mathbf{x} + \mathbf{n}_r, t), & \mathbf{x} + \mathbf{n}_r^- \geq 0 \\ 0, & \text{otherwise} \end{array} \right\} - \left\{ \begin{array}{cc} q_r(\mathbf{x}, t), & \mathbf{x} - \mathbf{n}_r^+ \geq 0 \\ 0, & \text{otherwise} \end{array} \right\}. \tag{3}$$

Summation of (3) over all $\mathbf{x}$ yields

$$\begin{aligned} \sum_{\mathbf{x} \in \mathbb{Z}_+^N} \frac{\partial p(\mathbf{x}, t)}{\partial t} &= \frac{\partial}{\partial t} \sum_{\mathbf{x} \in \mathbb{Z}_+^N} p(\mathbf{x}, t) = \sum_{\mathbf{x} + \mathbf{n}_r^- \geq 0} q(\mathbf{x} + \mathbf{n}_r, t) - \sum_{\mathbf{x} - \mathbf{n}_r^+ \geq 0} q(\mathbf{x}, t) \\ &= \sum_{\mathbf{y} \geq 0} q(\mathbf{y} + \mathbf{n}_r^+, t) - \sum_{\mathbf{y} \geq 0} q(\mathbf{y} + \mathbf{n}_r^+, t) = 0. \end{aligned} \tag{4}$$

Thus, the total probability $\sum_{\mathbf{x} \in \mathbb{Z}_+^N} p(\mathbf{x}, t)$ is constant over time and therefore conserved.

With R reactions the master equation is

$$\frac{\partial p(\mathbf{x}, t)}{\partial t} = \sum_{\substack{r=1 \\ \mathbf{x} + \mathbf{n}_r^- \geq 0}}^{R} q_r(\mathbf{x} + \mathbf{n}_r, t) - \sum_{\substack{r=1 \\ \mathbf{x} - \mathbf{n}_r^+ \geq 0}}^{R} q_r(\mathbf{x}, t). \tag{5}$$

It follows from (4) and (5) that the total probability in the master equation is also conserved.

By truncating the Taylor expansion of the first sum of the master equation (5) after the second order term we arrive at the FP equation [13] for $\mathbf{x} \in \mathbb{R}_+^N$.

The equation for the probability density is

$$\begin{aligned}\frac{\partial p(\mathbf{x},t)}{\partial t} &= \sum_{r=1}^{R}\left\{\sum_{i=1}^{N} n_{ri}\frac{\partial q_r(\mathbf{x},t)}{\partial x_i} + \sum_{i=1}^{N}\sum_{j=1}^{N}\frac{n_{ri}n_{rj}}{2}\frac{\partial^2 q_r(\mathbf{x},t)}{\partial x_i \partial x_j}\right\} \\ &= \sum_{r=1}^{R}\left\{\sum_{i=1}^{N} n_{ri}\frac{\partial}{\partial x_i}\left(q_r(\mathbf{x},t) + \frac{1}{2}\sum_{j=1}^{N} n_{rj}\frac{\partial q_r(\mathbf{x},t)}{\partial x_j}\right)\right\}.\end{aligned} \tag{6}$$

The conservation form of the FP equation is obtained by introducing $\mathbf{F}_r$ with the components

$$F_{ri} = n_{ri}(q_r + 0.5\mathbf{n}_r \cdot \nabla q_r),\ r = 1 \ldots R,\ i = 1 \ldots N.$$

Then by (6)

$$\frac{\partial p(\mathbf{x},t)}{\partial t} = \sum_{r=1}^{R} \nabla \cdot \mathbf{F}_r. \tag{7}$$

Assume that $p(\mathbf{x},t) = 0$ outside

$$\Omega(\rho) = \{\mathbf{x} \mid \mathbf{x} \in \mathbb{R}_+^N \text{ and } \|\mathbf{x}\|_2 < \rho\} \tag{8}$$

for some $\rho > 0$. Then $q_r = 0$ and $\mathbf{F}_r = 0$ in $\mathbb{R}_+^N \setminus \Omega(\rho)$ and the time derivative of the total probability in the non-negative orthant $\mathbb{R}_+^N$ is by Gauss' formula and (7)

$$\begin{aligned}\frac{\partial}{\partial t}\int_{\mathbb{R}_+^N} p(\mathbf{x},t)\,dV &= \int_{\mathbb{R}_+^N}\frac{\partial p}{\partial t}\,dV = \sum_{r=1}^{R}\int_{\mathbb{R}_+^N}\nabla\cdot\mathbf{F}_r\,dV = \sum_{r=1}^{R}\int_{\Omega}\nabla\cdot\mathbf{F}_r\,dV \\ &= \sum_{r=1}^{R}\int_{\partial\Omega}\mathbf{F}_r\cdot\mathbf{n}_\Omega\,dS = -\sum_{r=1}^{R}\sum_{i=1}^{N}\int_{\Gamma_i} F_{ri}\,dS \\ &= -\sum_{i=1}^{N}\int_{\Gamma_i}\sum_{r=1}^{R} n_{ri}(q_r + 0.5\mathbf{n}_r\cdot\nabla q_r)\,dS,\end{aligned} \tag{9}$$

where $\mathbf{n}_\Omega$ is the normal of $\partial\Omega$ and $\Gamma_i = \{\mathbf{x} \mid \mathbf{x} \in \mathbb{R}_+^N \text{ and } x_i = 0\}$. If the total flux in the FP equation satisfies

$$\sum_{r=1}^{R} n_{ri}(q_r + 0.5\mathbf{n}_r \cdot \nabla q_r) = 0 \ \text{ on } \ \Gamma_i,\ i = 1 \ldots N, \tag{10}$$

then the total probability in $\mathbb{R}_+^N$ is conserved. This is the boundary condition we adopt in the discretization of the FP equation in the next section.

In order to derive the adjoint equation for the space operator of the FP equation and its boundary condition from (6), consider for every r the inner product

$$\begin{aligned}
&\int_\Omega \mathbf{n}_r \cdot \nabla(q_r + 0.5\mathbf{n}_r \cdot q_r)u \; d\Omega \\
&= \int_{\partial\Omega} \mathbf{n}_\Omega \cdot \mathbf{n}_r(q_r + 0.5\mathbf{n}_r \cdot q_r)u \; dS - \int_\Omega p w_r(\mathbf{n}_r \cdot \nabla)u \; d\Omega \\
&-0.5\int_{\partial\Omega} \mathbf{n}_\Omega \cdot \mathbf{n}_r q_r \nabla \cdot (\mathbf{n}_r u) \; dS + 0.5\int_\Omega p w_r(\mathbf{n}_r \cdot \nabla)\nabla \cdot (\mathbf{n}_r u) \; d\Omega.
\end{aligned}$$

Since $\sum_r \mathbf{n}_r(q_r + 0.5\mathbf{n}_r \cdot q_r) = 0$ on $\partial\Omega$, the adjoint equation and its boundary condition are

$$\begin{aligned}
\sum_{r=1}^{R} w_r \sum_{i=1}^{N} n_{ri} \left\{ \frac{\partial u}{\partial x_i} - 0.5 \sum_{j=1}^{N} n_{rj} \frac{\partial^2 u}{\partial x_i \partial x_j} \right\} &= 0, \\
\sum_{r=1}^{R} n_{ri} w_r \sum_{j=1}^{N} n_{rj} \frac{\partial u}{\partial x_j} &= 0 \text{ on } \Gamma_i.
\end{aligned} \tag{11}$$

A solution to (11) is a constant u. This solution is compared to the solution of the discretized adjoint equation in Sect. 5.

3 Discretization

A numerical method for solution of the FP equation (7) with the boundary conditions (10) is described in this section. The method is adaptive in space and time and the total probability is preserved as it is in the analytical counterpart (9).

3.1 Space discretization

The FP equation (7) is discretized by a finite volume method in 2D with quadrilateral cells as in [9]. Integrate (7) using Gauss' theorem over one cell ω_{ij} in $\mathbb{R}^2_+$ to obtain

$$\frac{\partial p_{ij}}{\partial t} = \frac{1}{|\omega_{ij}|}\int_{\omega_{ij}} \frac{\partial p(\mathbf{x},t)}{\partial t} \; d\omega = \frac{1}{|\omega_{ij}|}\int_{\omega_{ij}} \sum_{r=1}^{R} \nabla \cdot \mathbf{F}_r \; d\omega = \frac{1}{|\omega_{ij}|}\int_{\partial\omega_{ij}} \mathbf{F} \cdot \mathbf{n}_\omega \; dS, \tag{12}$$

where p_{ij} is the average in a cell, $\mathbf{F} = \sum_{r=1}^{R} \mathbf{F}_r$, and $\mathbf{n}_\omega$ is the normal on the boundary $\partial\omega_{ij}$ of cell ω_{ij} with area $|\omega_{ij}|$.

For evaluation of the integral on $\partial\omega_{ij}$, we need an approximation of $\mathbf{F} = \sum_{r=1}^{R} \mathbf{n}_r(q_r + 0.5\mathbf{n}_r \cdot \nabla q_r)$ using the cell averages p_{ij}. An upwind approximation

of $\sum_{r=1}^{R} n_{ri}q_r$ is chosen depending on the sign of w in

$$\sum_{r=1}^{R} n_{ri}q_r = \sum_{r=1}^{R} n_{ri}w_r p = wp.$$

On the face $(i+1/2, j)$ between ω_{ij} and $\omega_{i+1,j}$

$$\sum_{r=1}^{R} n_{ri}q_r = \begin{cases} w_{i+1/2,j}(3p_{ij} - p_{i-1,j})/2, & w_{i+1/2,j} < 0, \\ w_{i+1/2,j}(3p_{i+1,j} - p_{i+2,j})/2, & w_{i+1/2,j} \geq 0. \end{cases} \tag{13}$$

The gradient is approximated in a dual grid with cell corners at the midpoints of the primal grid. By Gauss' theorem in a dual cell $\omega_{i+1/2,j+1/2}$ with midpoint at the common corner of ω_{ij} and $\omega_{i+1,j+1}$

$$\begin{aligned} \nabla q_{i+1/2,j+1/2} &= \frac{1}{|\omega_{i+1/2,j+1/2}|} \int_{\omega_{i+1/2,j+1/2}} \nabla q \, d\omega \\ &= \frac{1}{|\omega_{i+1/2,j+1/2}|} \int_{\partial\omega_{i+1/2,j+1/2}} q\mathbf{n}_\omega dS. \end{aligned}$$

Then q is approximated at the right hand face of $\omega_{i+1/2,j+1/2}$ by $0.5(q_{i+1,j} + q_{i+1,j+1})$. The other cell faces are treated similarly. Finally, on the face $(i+1/2, j)$

$$\nabla q_{i+1/2,j} = 0.5(\nabla q_{i+1/2,j+1/2} + \nabla q_{i+1/2,j-1/2}).$$

The approximation on the other cell faces of ω_{ij} is the same. The scheme is second order accurate on grids with constant grid size. In conclusion, the time dependent equation for p_{ij} in a rectangular cell with the length of the edges Δx and Δy in a rectangular domain Ω is

$$\begin{aligned} \frac{dp_{ij}}{dt} &= \Phi_{ij}(\mathbf{p}) = \tfrac{1}{|\omega_{ij}|}\big((\mathbf{F}_{i+1/2,j} - \mathbf{F}_{i-1/2,j})\Delta y + (\mathbf{F}_{i,j+1/2} - \mathbf{F}_{i,j-1/2})\Delta x\big), \\ & i = 1, \ldots, N_i, \ j = 1, \ldots, N_j. \end{aligned} \tag{14}$$

The vector $\mathbf{p}$ consists of all the averages p_{ij} in some order.

The master equation in 1D for two reactions is compared to the discretization of the FP equation. Let the cells be $\omega_i = \{i - 1/2 \leq x < i + 1/2\}$, $i = 0, 1, 2 \ldots$, and suppose that $n_1 = 1$ and $n_2 = -1$. Then

$$(q_1 + 0.5\frac{\partial q_1}{\partial x})(i) \approx q_1(i + 1/2), \; (q_2 - 0.5\frac{\partial q_2}{\partial x})(i) \approx q_2(i - 1/2),$$

and the master equation is

$$\frac{\partial p_i}{\partial t} = q_{1,i+1} - q_{1,i} + q_{2,i-1} - q_{2,i}, \; i \geq 1, \; \frac{\partial p_0}{\partial t} = q_{1,1} - q_{1,0} - q_{2,0}. \tag{15}$$

The finite volume approximation of the FP equation is

$$\begin{aligned}\frac{\partial p_i}{\partial t} &\approx I_{i-1/2}^{i+1/2}(q_1(i+1/2) - q_2(i-1/2)) = q_{1,i+1} - q_{1,i} + q_{2,i-1} - q_{2,i}, i \geq 1,\\ \frac{\partial p_0}{\partial t} &\approx q_{1,1} - q_{1,0} - q_{2,0}.\end{aligned} \tag{16}$$

The right hand sides in (15) and (16) are identical, also at the boundary.

The stability of the space discretization can be investigated with the model equation in 1D

$$a\frac{\partial p}{\partial x} + b\frac{\partial^2 p}{\partial x^2} = 0,$$

where a and b are positive and constant. With a centered evaluation $0.5w_{i+1/2}(p_{i+1}+p_i)$ in (13) instead of the upwind flux, the discrete solution is non-oscillatory only if Δx is so small that the cell Peclet number satisfies $a\Delta x/(2b) \leq 1$ [17]. For the upwind scheme in (13) the discrete solution is

$$p_i = \sum_{k=1}^{3} \gamma_k \lambda_k^i,\ \lambda_1 = 1,\ \lambda_{2,3} = \alpha \pm \sqrt{\alpha^2 - \beta},$$

where $\alpha = (3a\Delta x + 2b)/(2a\Delta x)$ and $\beta = 2b/(a\Delta x)$. Since $\beta > 0$ and $\alpha^2 - \beta > 0$ we have $\lambda_{2,3} > 0$ and no oscillations occur in this case.

3.2 Grid structure and interpolation

The computational domain is a rectangle $[0, x_{max}] \times [0, y_{max}]$ with $x_{max}, y_{max} > \rho$ in (8). It is covered by a Cartesian grid partitioned into blocks as in [8, 16]. A block consists of a number of cells and the cell size is adapted so that the estimated spatial error in the solution is sufficiently small. All cells in a block are refined if at least one cell is flagged for refinement. All cells in a block are coarsened if this is acceptable for the error in all the cells. The coarsening and refinement are introduced by doubling or halving the grid size. The jump in grid size at the boundary between two blocks is at most two.

Each block has a layer of ghost cells outside the block to simplify the application of the discretization stencil in a block and the communication of data between the blocks. Two layers of extra cells are needed for our space discretization. If the grid size is the same on both sides of a block boundary, then the cell values in one block are copied into the corresponding ghost cells in the other block. If a ghost cell ω_{IJ} corresponds to four cells $\omega_{ij}, \omega_{i+1,j}, \omega_{i,j+1}, \omega_{i+1,j+1}$ in the adjacent block, then the value in the ghost cell is updated by the area weighted

average in the four cells so that the restriction is

$$p_{IJ} = r_{IJ}(\mathbf{p}) = \sum_{k=i}^{i+1}\sum_{l=j}^{j+1} \kappa_{kl} p_{kl}, \kappa_{ij} = |\omega_{ij}| / \sum_{k=i}^{i+1}\sum_{l=j}^{j+1} |\omega_{kl}|. \tag{17}$$

If four ghost cells cover one cell in the coarse block, then the values in the ghost cells are determined by accurate interpolation.

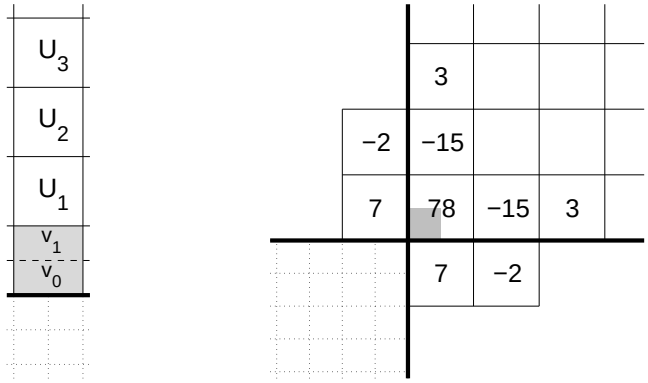

(a) (b)

Figure 1: Interpolation molecules at the block boundaries. (a) The shaded cell is split into two parts for one-sided interpolation in the normal direction. (b) Interpolation weights multiplied by 64 for the shaded diagonal ghost cell at a block corner.

The prolongation from a coarse cell to the corresponding four ghost cells in the fine grid has to be fourth order accurate for second order accuracy in the approximation of the second derivatives [9]. In Fig. 1.a, the upper coarse grid block shares a block boundary with the lower fine grid block. The shaded coarse cell consists of four fine ghost cells. They are updated by one-sided interpolation from the coarse cells. One-sided interpolation is necessary for stability at the block interfaces in [9, 16]. Firstly, U_0 in the coarse cells along the boundary is split into two parts (see Fig. 1.a)

$$v_0 = U_0 - d_0,\ v_1 = U_0 + d_0,\ d_0 = (29\,U_0 - 47\,U_1 + 23\,U_2 - 5\,U_3)/64.$$

Then the coarse cells are split vertically and the values in the lower and upper row along the boundary, v_{0i} and v_{1i}, are prolongated to the left and right values w_{00i} and w_{01i} in the lower row and to the left and right values w_{10i} and w_{11i} in the upper row. The interpolation is

$$\begin{aligned} &w_{j0i} = v_{ji} - d_{ji},\ w_{j1i} = v_{ji} + d_{ji}, j = 0, 1, \\ &d_{ji} = \tfrac{11}{64}(v_{j,i+1} - v_{j,i-1}) - \tfrac{3}{128}(v_{j,i+2} - v_{j,i-2}). \end{aligned} \tag{18}$$

In this manner, the w-values in the fine ghost cells are determined from the U-values in the coarse cells to fourth order accuracy. The advantage of coordinate splitting of the prolongation is simplicity, few operations and convenient generalization to multi-dimensions. The interpolation (18) is also employed in both coordinate directions for transfering values in the inner cells of a block when the grid is refined. The value in the coarse cell is preserved locally since

$$\sum_{j=0,1} w_{j0} + w_{j1} = \sum_{j=0,1} v_j = U_0 - d_0 + U_0 + d_0 = U_0.$$

The diagonal ghost cell at a block corner, see Fig. 1.b, is needed for the approximation of second order derivatives, and the data for these ghost cells are obtained from the diagonally located neighboring block. The value in the shaded fine ghost cell is calculated by interpolation with the coefficients in the figure.

The centered interpolation operator (18) use ghost cell data at the ends of the interface. For these to be available, we must update the ghost cells in a certain order. First copy at interfaces without jumps in grid size, and restrict from fine to coarse ghost cells. Then fine ghost cells are filled in from coarser block data. The interpolation is finished by updating all diagonal ghost cells.

3.3 Time discretization

After space discretization, write the time dependent equations as

$$\frac{d\mathbf{p}}{dt} = A\mathbf{p}. \tag{19}$$

The matrix A is constant for a given grid. The time derivative is approximated by the backward differentiation formula of order two (BDF-2). To advance the solution $\mathbf{p}^{n-1}$ at t^{n-1} to t^n with a variable time step $\Delta t^n = t^n - t^{n-1}$, $\mathbf{p}^n$ is updated by

$$(\alpha_0^n I - \Delta t^n A)\mathbf{p}^n = -\alpha_1^n \mathbf{p}^{n-1} - \alpha_2^n \mathbf{p}^{n-2}. \tag{20}$$

The coefficients in (19) are [12, 16]

$$\begin{aligned} &\theta^n = \Delta t_n / \Delta t_{n-1}, \\ &\alpha_0^n = (1+2\theta^n)/(1+\theta^n),\ \alpha_1^n = -(1+\theta^n),\ \alpha_2^n = (\theta^n)^2/(1+\theta^n). \end{aligned} \tag{21}$$

The integration is initialized at $t^0 = 0$ by the Euler backward method.

Assume that A is diagonalizable, that Z has the eigenvectors $\mathbf{z}_k$ as columns, and that Λ has the eigenvalues λ_k in the diagonal so that $A = Z\Lambda Z^{-1}$. Introduce $\mathbf{s}^n = Z^{-1}\mathbf{p}^n$ in (20) to arrive at

$$\alpha_0^n \mathbf{s}^n + \alpha_1^n \mathbf{s}^{n-1} + \alpha_2^n \mathbf{s}^{n-2} = \Delta t \Lambda \mathbf{s}^n. \tag{22}$$

Let the time step Δt be constant for simplicity so that $\alpha_0 = 3/2, \alpha_1 = -2, \alpha_2 = 1/2$. The k:th component in $\mathbf{s}^n$ is a solution to the difference equation (22) with λ_k replacing Λ

$$\begin{aligned} &s_k^n = \gamma_{1k}^n s_k^0 + \gamma_{2k}^n s_k^1,\ n \geq 0, \\ &\gamma_{1k} = (1+\beta_1)/\beta_2,\ \gamma_{2k} = (1-\beta_1)/\beta_2, \\ &\beta_1 = 0.5\sqrt{1+2\Delta t\lambda_k},\ \beta_2 = 1.5 - \Delta t\lambda_k. \end{aligned} \tag{23}$$

For a sufficiently small $\Delta t\lambda_k$, s_k^n is dominated by its first term in (23) for increasing n and

$$\gamma_{1k} = 1 + \Delta t\lambda_k + \mathcal{O}(|\Delta t\lambda_k|^2). \tag{24}$$

If $\Re\lambda_k < 0$ but small, then there is a Δt such that $|\gamma_{1k}| < 1$ and s_k^n vanishes when $n \to \infty$ but the decay may be slow.

The system of linear equations (20) is solved in each time step by restarted GMRES [18].

3.4 Conservation

The discrete total probability P is defined by (cf. Sect. 2)

$$P = \sum_{\omega_{ij} \in \Omega} |\omega_{ij}| p_{ij}. \tag{25}$$

By summing $|\omega_{ij}|p_{ij}$ over all $N_i N_j$ cells in (14) and taking into account that $\mathbf{F}_{1/2,j} = \mathbf{F}_{i,1/2} = 0$ by the boundary condition (11) and that $p = 0$ at the outer boundary and therefore $\mathbf{F}_{N_i+1/2,j} = \mathbf{F}_{i,N_j+1/2} = 0$, we have that $dP/dt = 0$ and the total probability is preserved.

This also holds true on a grid with blocks and block interfaces with equal grid size on both sides. If two cell faces on one side meet one face on the other side of the interface, then the average of the two fine grid fluxes will in general not be equal to the coarse grid flux. For the flux to be unique there, the average from the fine grid is chosen for the coarse cell. It is shown in [16] that one order of accuracy is lost locally by this procedure. Extra precautions are necessary at the corners where coinciding ghost cells of different blocks may be filled with different data.

Let A be the space discretization matrix resulting from a conservative scheme and let $\mathbf{w}$ be the vector of all cell areas $|\omega_{ij}|$ ordered in the same way as p_{ij} in $\mathbf{p}$. Then by (20)

$$\begin{aligned} 0 = \Delta t^n \mathbf{w}^T A \mathbf{p}^n &= \alpha_0^n \mathbf{w}^T \mathbf{p}^n + \alpha_1^n \mathbf{w}^T \mathbf{p}^{n-1} + \alpha_2^n \mathbf{w}^T \mathbf{p}^{n-2} \\ &= \alpha_0^n P^n + \alpha_1^n P^{n-1} + \alpha_2^n P^{n-2}. \end{aligned} \tag{26}$$

If $0 < \theta^n < 1 + \sqrt{2}$ for θ^n in (21), then BDF-2 is stable [12] implying that the recursion for P^n in (26) is stable. If $P^0 = P^1 = 1$, then $P^n = 1$ for all n, since $\alpha_0^n + \alpha_1^n + \alpha_2^n = 0$.

4 Error control

The grid size in a block is determined by an estimated spatial discretization error. The time step is chosen such that the estimated temporal error is sufficiently small. If a finer grid is necessary, then the solution is interpolated from the present grid to the finer grid so that the total probability P in (25) is preserved.

The discretization error caused by the finite volume approximation is estimated by comparing the space operator Φ in (14) on a coarse and a fine grid. A cell in the coarse grid is formed by merging the corresponding four cells in the fine grid as in [8, 16], and (17). The restriction of Φ on the fine grid is compared to Φ on the coarse grid applied to the restriction of the fine grid solution for the error estimate τ_S in all the four fine grid cells

$$\tau_S = \frac{1}{3}(r(\Phi(\mathbf{p})) - \Phi(r(\mathbf{p}))). \tag{27}$$

If $|\tau_{Sij}| > \epsilon_S$ in at least one cell ij in a block, then all cells in that block are refined by halving the grid size. New solution values are obtained by conservative prolongation (18). If $|\tau_{Sij}| < \epsilon_S/20$ for all cells in a block then the grid size is doubled in that block and new p_{ij} are computed with the restriction (17).

The error due to the time stepping scheme is estimated by comparing $\mathbf{p}^n$ from (20) with an explicit predictor using $\mathbf{p}^{n-1}$ and $\mathbf{p}^{n-2}$ of second order as in [16]. The maximum of the estimates τ_{Tij} in all cells is compared to the tolerance ϵ_T in

$$\zeta = \sqrt{\epsilon_T/|\tau_T|_\infty}. \tag{28}$$

A step is accepted if $1 \leq \zeta \leq 1.1$ and $\Delta t_{n+1} = \Delta t_n$. The step is rejected if $\zeta < 1$ and recomputed with $\Delta t_n := 0.9\zeta\Delta t_n$. If $\zeta > 1.1$, then the step is accepted and the time step increased with $\Delta t_{n+1} = 1.1\Delta t_n$.

An upper bound is introduced on Δt to avoid slow convergence in the GMRES-iterations. Either it is a fixed bound or it is given by a CFL-number χ of $\mathcal{O}(1)$ and the minimal Δx in the grid

$$\Delta t_{max} = \chi\Delta x_{min}. \tag{29}$$

The size of the spectrum of the iteration matrix $I - \Delta t A$ grows linearly when Δt grows and a deteriorating performance of the iterative solver is the usual result without the bound Δt_{max}.

5 Steady state solution

The discrete steady state solution $\mathbf{p}^\infty$ satisfies

$$A\mathbf{p}^\infty = 0, \tag{30}$$

when the time derivatives have vanished. The stationary $\mathbf{p}^\infty$ can be calculated as the eigenvector of A corresponding to the zero eigenvalue. Such an eigenvalue always exists in a conservative method as is shown by considering (26) and the fact that $\mathbf{w}^T A\mathbf{p} = 0$ for the area vector $\mathbf{w}$ and all $\mathbf{p}$. Therefore, $\mathbf{w}^T A = 0$ and $\mathbf{w}$ is the left eigenvector of A with eigenvalue zero and $\mathbf{p}^\infty$ is the right eigenvector of the same eigenvalue. Then we have proved

Proposition *If A is defined by a conservative method, then there is a steady state solution and it is the right eigenvector corresponding to the zero eigenvalue of A.*

The adjoint steady state equation of the discretization $A^T\mathbf{u} = 0$ has the solution $\mathbf{u} = \mathbf{w}$. If the grid size is constant, then w_{ij} is constant. This is also the solution to the adjoint of the analytical FP equation (11).

A good algorithm to compute a few small eigenvalues and their eigenvectors of a large, sparse matrix A is the implicitly restarted Arnoldi method for non-symmetric matrices implemented in ARPACK [15]. The eigenvector is computed by successively refining the grid starting with a coarse, uniform grid with matrix A_0. The spatial error in $\mathbf{p}_k^\infty$ on grid k with matrix A_k is estimated as in (27) and the blocks are refined or coarsened using the same criteria as in the time stepping algorithm. The new grid $k+1$ and A_{k+1} are generated and a new eigenvector $\mathbf{p}_{k+1}^\infty$ is computed. The iteration is terminated when the estimated error is less than ϵ_S.

An alternative is to integrate (19) forward in time until the residual $A\mathbf{p}$ is sufficiently small. When $\lambda_1 = 0$ in (22) and (23) we have

$$s_1^n = s_1^0 + 3^{-n} s_1^1.$$

If $\Re\lambda_j \le \varepsilon < 0,\ j \ge 2$, then all other components s_j^n vanish by the stability properties of BDF-2 [12]. Consequently,

$$\lim_{n\to\infty} \mathbf{p}^n = \lim_{n\to\infty} Z\mathbf{s}^n = \mathbf{z}_1 s_1^0,$$

but as remarked in the end of Sect. 3.3 the convergence is often slow since ε is small and this is confirmed in the numerical examples in Sect. 6.

For a non-conservative scheme, the smallest eigenvalue λ_1 of A may have $\Re\lambda_1 > 0$ but $\Re\lambda_j < 0$ for $j \ge 2$. By (22) and (23) the dominant term in $\mathbf{p}^n$ for large n is growing slowly

$$\mathbf{p}^n \approx (1 + \Delta t\lambda_1)^n \mathbf{z}_1.$$

Since $\mathbf{w}$ is an approximation of the first row of Z^{-1}, we have $\mathbf{w}^T\mathbf{z}_1 \approx 1$ and

$$P^n = \mathbf{w}^T\mathbf{p}^n \approx (1 + \Delta t\lambda_1)^n. \tag{31}$$

The total probability also exhibits a slow growth. This growth is avoided by rescaling $\mathbf{p}^n$ occasionally by

$$\mathbf{p}^n := \frac{P^0}{\mathbf{w}^T\mathbf{p}^n}\mathbf{p}^n, \tag{32}$$

so that P^n remains constant and $\mathbf{p}^n$ is stabilized. Since the boundary conditions (10) are homogeneous and the FP equation (6) and its discretization are linear and homogeneous, the new $\mathbf{p}^n$ is also a solution.

6 Numerical results

Our method for solution of the FP equation is applied to two different systems with two molecular species as in [7, 20]. The time-dependent and steady state solutions are computed by the time-stepping scheme and by calculating the eigenvector with eigenvalue zero. In the second example, the solution is compared to Gillespie's stochastic method [10]. The solutions are scaled such that $|p|_\infty = 1$ initially.

6.1 Metabolite reactions

Consider the following five reactions for the molecular species X and Y modeling the creation of two metabolites controled by two enzymes, a reaction and their destruction:

$$\begin{array}{ll} \emptyset \xrightarrow{k_X} X & \emptyset \xrightarrow{k_Y} Y \\ X + Y \xrightarrow{k_2[x][y]} \emptyset & \\ X \xrightarrow{\mu[x]} \emptyset & Y \xrightarrow{\mu[y]} \emptyset \end{array}$$

The difference between the states and the propensities for the five reactions are

$$\begin{array}{llll} \mathbf{n}_1^T = (-1,0), & w_1 = k_X, & \mathbf{n}_2^T = (0,-1), & w_2 = k_Y, \\ \mathbf{n}_3^T = (1,1), & w_3 = k_2 xy, & \mathbf{n}_4^T = (1,0), & w_4 = \mu x, \\ \mathbf{n}_5^T = (0,1), & w_5 = \mu y. & & \end{array} \tag{33}$$

The corresponding FP equation is (cf. (6))

$$\begin{aligned} \frac{\partial\, p(x,y,t)}{\partial\, t} &= k_X(-p_x + 0.5p_{xx}) + k_Y(-p_y + 0.5p_{yy}) \\ &+ \mu((xp)_x + 0.5(xp)_{xx} + (yp)_y + 0.5(yp)_{yy}) \\ &+ k_2((xyp)_x + (xyp)_y + 0.5(xyp)_{xx} + (xyp)_{xy} + 0.5(xyp)_{yy}). \end{aligned}$$

In the experiments, the coefficients are $k_X = k_Y = 0.6$ and $\mu = k_2 = 0.001$, and the computational domain is the square $\Omega = \{0 \le x, y \le 200\}$.

The computational domain is partitioned into 8×8 blocks. The error tolerances for the adaptation in space and time are $\epsilon_S = \epsilon_T = .003$. The initial distribution is a Gauss pulse at $x = y = 60$ and is displayed in Fig. 2.a together with the first adapted grid. Every 8:th grid line is drawn in each space dimension in the figures. The solution propagates towards a steady state in the lower left corner, see Fig. 2.b.

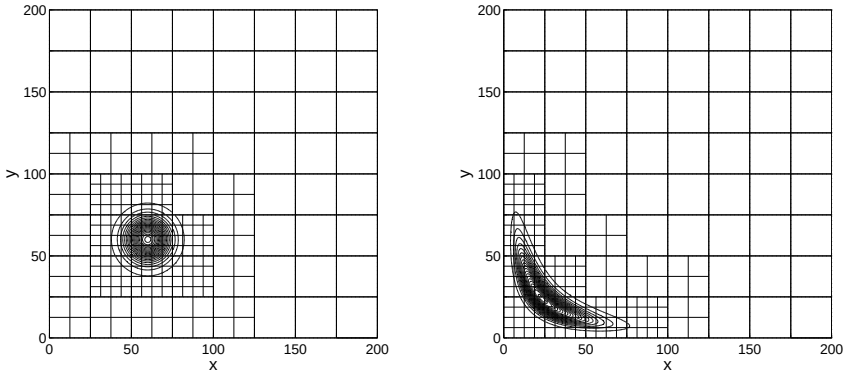

(a) (b)

Figure 2: The initial solution (a), and the solution after $5 \cdot 10^4$ time steps (b).

The equation is integrated for $5 \cdot 10^4$ time steps corresponding to a final time $T = 8742$. The time histories of the number of cells and the time steps are found in Fig. 3. After about 4400 steps the number of cells is constant when the solution approaches the steady state. The time step increases in the beginning of the time interval and reaches its maximum value Δt_{max}. Close to the stationary solution the time steps can be large and still be accurate but the convergence of the iterative solver will be poor if Δt is allowed to increase too much (see Sect. 4).

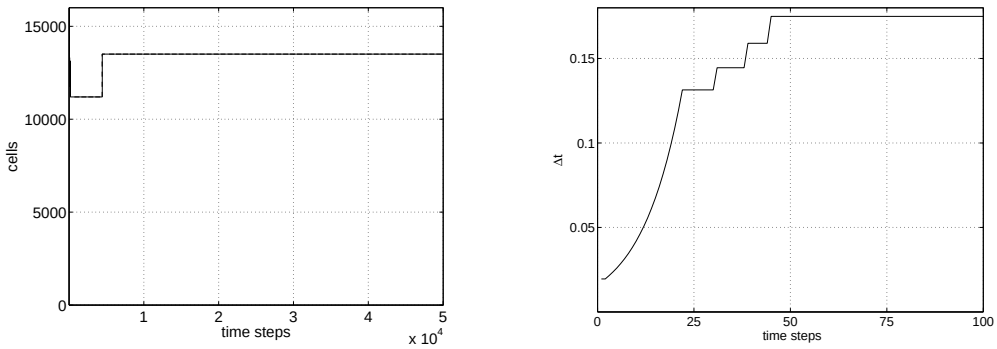

(a) (b)

Figure 3: Time series of the number of cells (a), and the length of the initial time steps (b).

The problem is solved with and without conservation at block interfaces. Let the discretization matrix on the final grid with conservation be A_c and without conservation A_{nc}. The time evolution of the residuals $A\mathbf{p}^n$ of the two discretizations are displayed in Fig. 4.a. The residual $|A_c\mathbf{p}^n|_\infty$ decays steadily but $|A_{nc}\mathbf{p}^n|_\infty$ stagnates at about $6 \cdot 10^{-6}$. The explanation is that A_c has a computed eigenvalue $\lambda_{min}(A_c) = 3 \cdot 10^{-17}$ and for A_{nc} the smallest eigenvalue is $\lambda_{min}(A_{nc}) = 6.3 \cdot 10^{-6}$. Then $\mathbf{p}^n \rightarrow \mathbf{p}_{nc}^\infty$ where $\mathbf{p}_{nc}^\infty$ is the eigenvector of the smallest eigenvalue and

$|\mathbf{p}_{nc}^{\infty}|_\infty \approx 0.95$. Thus, $|A_{nc}\mathbf{p}^n|_\infty \to \lambda_{min}(A_{nc})|\mathbf{p}_{nc}^{\infty}|_\infty \approx 0.95\lambda_{min}(A_{nc})$ which is in good agreement with the stagnated residual in Fig. 4.a. The sudden increase in the residual at about 4400 time steps is explained by the change of grid size in Fig. 3.a.

There is no steady state solution in the non-conservative case except for the trivial $\mathbf{p} = 0$ and the growth of $\mathbf{p}_{nc}^{\infty}$ is according to (24) approximately

$$(\gamma_{11})^n \approx \exp(\lambda_{min}(A_{nc})n\Delta t).$$

Thus, with $n = 5 \cdot 10^4$ and $\Delta t = 0.17$ from Fig. 3.b the growth factor is 1.055. The scaled total probability P^n/P^0 is preserved with conservation in Fig. 4.b but it grows slowly without a conservative scheme. The measured increase in P^n/P^0 is 5 per cent as expected from (31). The difference between the solutions at $5 \cdot 10^4$ time steps obtained with A_c and with A_{nc} with rescaling of $\mathbf{p}^n$ as in (32) is shown in Fig. 5.a. The maximal difference is 0.18 per cent of $|\mathbf{p}|_\infty$.

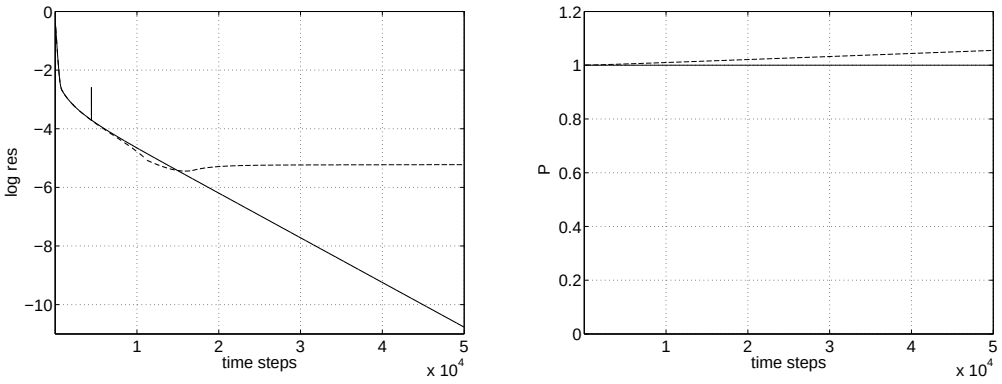

(a) (b)

Figure 4: Time series for the conservative (solid) and the non-conservative (dashed) schemes. (a) The logarithm of the residual. (b) Conservation of total probability.

The steady state solution is computed as the eigenvector of A_c with eigenvalue zero (see Sect. 5). The zero eigensolution is computed on three successively refined grids. The third grid is identical to the grid obtained with the time stepping scheme after about 4400 steps. One iteration with the Arnoldi implementation in *eigs* in MATLAB is sufficient at each grid level and every iteration requires 20 solutions of systems of linear equations with the system matrix $A_c - \sigma I$, where σ is 10^{-5}. The initial dimension of the matrix is about 4000 and on the final grid it is about 13300.

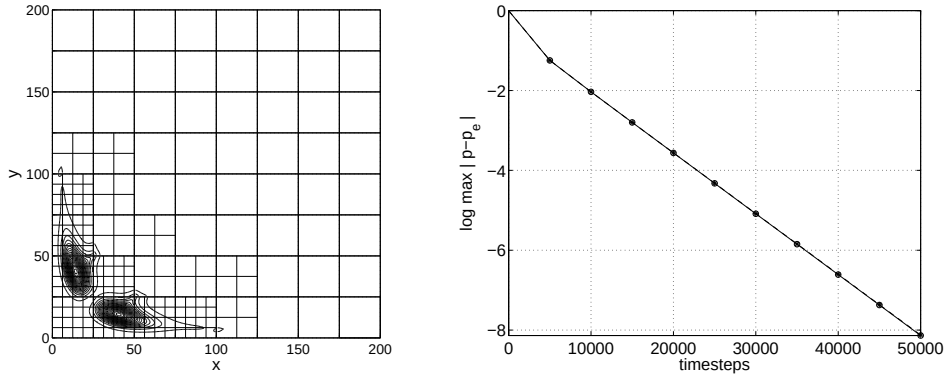

(a) (b)

Figure 5: The difference between the solutions with and without conservation at block interfaces after rescaling. (a) At $5 \cdot 10^4$ time steps. (b) The logarithm of the maximum difference between the zero eigenvector and the time dependent solutions.

The maximal difference between the steady state solution and the time dependent solutions with A_c and A_{nc} during $5 \cdot 10^4$ time steps is found in Fig. 5.b. The non-conservative solution is rescaled as in (32) afterwards at every 5000:th time step. The difference in convergence using conservation and a rescaled non-conservative solution is not visible in the plot. A conservative scheme and an adjustment of the probability with a non-conservative scheme yield similar results for the probability even though the residuals do not agree very well in Fig. 4.b. This is explained by the difference between A_c and A_{nc}.

At least one solution of a system of linear equations with the matrix $\alpha_0^n I - \Delta t A$ is necessary in each time step of the time integration algorithm. Hence, more than $5 \cdot 10^4$ solutions are computed to determine the stationary solution while only 60 solutions with $A_c - \sigma I$ are needed with the eigenvalue routine.

6.2 Circadian rhythm

Many different organisms have developed biological clocks to regulate the biochemistry of their cells to best suit e.g. the daily variations in light. A model for the circadian rhythm is derived by Vilar et al [20] from [1] taking the biochemical noise into account. A wide variety of different organisms seems to use similar mechanisms to produce reliable chemical oscillations [4]. The model has two molecular species, the complex X and the repressor Y. It is shown in [20] that the deterministic model (2) with certain parameters fails to exhibit a periodic behavior but the solution of the stochastic model (5) is periodic. The reason is that the deterministic solution reaches a stable fixed point and stays there while the noise in the stochastic solution is a sufficient perturbation for it to remain cyclic for many periods.

The difference between the states and the propensities of the four reactions in the model in [20] are

$$\begin{array}{lcll} \mathbf{n}_1^T & = & (0,-1), & w_1 = \beta_R(\alpha_R\theta_R + \alpha'_R\gamma_R\tilde{A}(y)))/(\delta_{MR}(\theta_R + \gamma_R\tilde{A}(y))), \\ \mathbf{n}_2^T & = & (0,1), & w_2 = \delta_R y, \\ \mathbf{n}_3^T & = & (-1,1), & w_3 = \gamma_C\tilde{A}(y)y, \\ \mathbf{n}_4^T & = & (1,-1), & w_4 = \delta_A x, \end{array} \tag{34}$$

where

$$\begin{array}{lcl} \tilde{A}(y) & = & 0.5(\alpha'_A\rho(y) - K_d + \sqrt{(\alpha'_A\rho(y) - K_d)^2 + 4\alpha_A\rho(y)K_d}), \\ \rho(y) & = & \beta_A/(\delta_{MA}(\gamma_C y + \delta_A)), K_d = \theta_A/\gamma_A. \end{array}$$

The FP equation is then

$$\begin{array}{rcl} \dfrac{\partial\, p(x,y,t)}{\partial\, t} & = & -(w_1p)_x + 0.5(w_1p)_{xx} + (w_2p)_y + 0.5(w_2p)_{yy} \\ & - & (w_3p)_x + (w_3p)_y + 0.5(w_3p)_{xx} - (w_3p)_{xy} + 0.5(w_3p)_{yy} \\ & + & (w_4p)_x - (w_4p)_y + 0.5(w_4p)_{xx} - (w_4p)_{xy} + 0.5(w_4p)_{yy}. \end{array} \tag{35}$$

The coefficients of the model in the numerical experiments are:

α_A	50	β_A	50	γ_A	1	δ_A	1	θ_A	50
α_R	0.01	β_R	5	γ_C	1	δ_R	0.2	θ_R	100
α'_A	500			γ_R	1	δ_{MA}	10		
α'_R	50					δ_{MR}	0.5		

The computational domain $\Omega = \{0 \le x \le 2500\ , 0 \le y \le 2000\}$ is initially partitioned into 10×10 blocks. The grid is stretched in the y-direction close to the x-axis. The error tolerances are $\epsilon_S = 0.01$ and $\epsilon_T = 0.01$ with $\chi = 7$ in (29) and the initial solution is a Gauss pulse at $(750, 600)$. The FP equation (35) is integrated until a final time at about $T = 370$ with the total probability conserved.

For comparison with the FP solution, M trajectories are generated with Gillespie's method [10]. Each trajectory simulates the time evolution of the chemical system modeled by the master equation (5). The state of the system is advanced in time by first deciding when the next reaction will take place and then which reaction it will be. These two numbers are drawn from two probability distributions. Then the state is updated and one time step has been completed. The solution domain is first divided into boxes $B_{ij} = \{(i-1)d \le x < id, (j-1)d \le y < jd\}, i, j = 1, 2, 3, \ldots$ for some $d > 0$. Then at given times $t_1, t_2, \ldots$ the number of trajectories m_{ij} with the solution in a box B_{ij} is counted and the estimate of the probability is $p_{ij}(t_k) = m_{ij}/M$. In the results below, we choose $d = 10$. By computing the probability in boxes, the work and storage grow exponentially with the dimension N of the problem also for this method.

The maximum of the solutions is displayed in Fig. 6. The solution is oscillatory with an average period of 14.3 for the FP equation and a few per cent longer with Gillespie's Monte Carlo (MC) method.

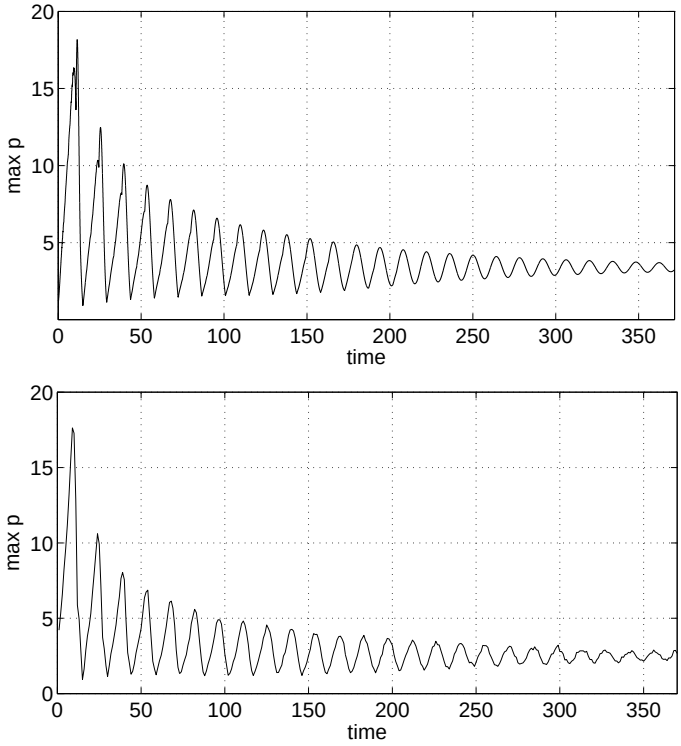

Figure 6: The variation of the maximum of the FP solution (upper) and the MC solution for $M = 10^5$ (lower).

The deterministic FP solution and its grid and p_{ij} obtained with the stochastic method with $M = 10^6$ are collected in Fig. 7 at $t_k = 23.76, 27.52, 31.08, 34.62$. The probability mass rotates in the counter-clockwise direction with a high speed at about $t = 27$ and a slow speed in the beginning and the end of the period. The trajectories in the MC solution are initialized by randomly choosing a point in the positive quadrant with the same probability as the initial solution of the FP equation.

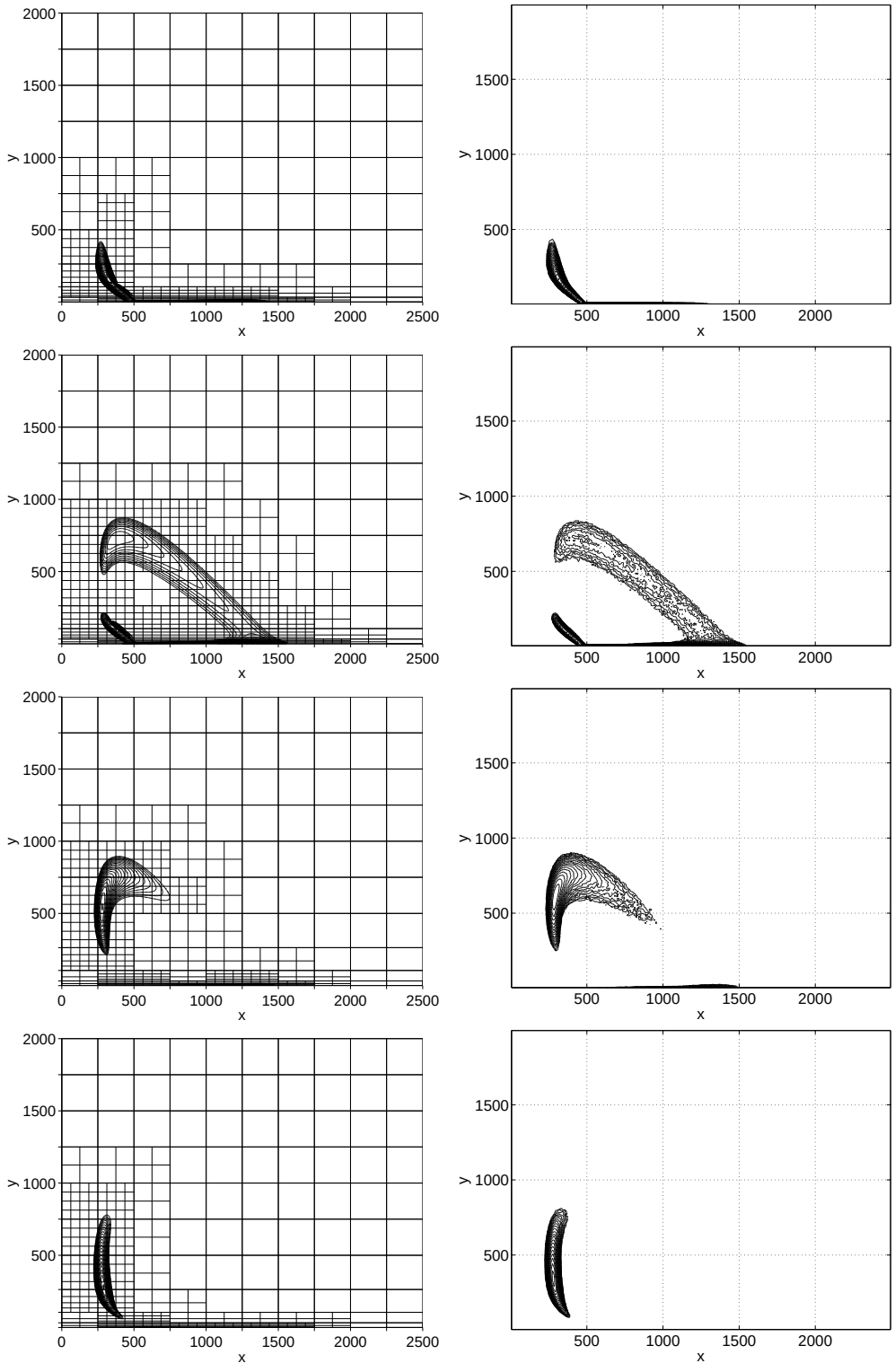

Figure 7: Isolines in a logarithmic scale at t=23.76, 27.52, 31.08, and 34.62 (from top to bottom) for the FP solution (left) and the MC solution with $M = 10^6$ (right).

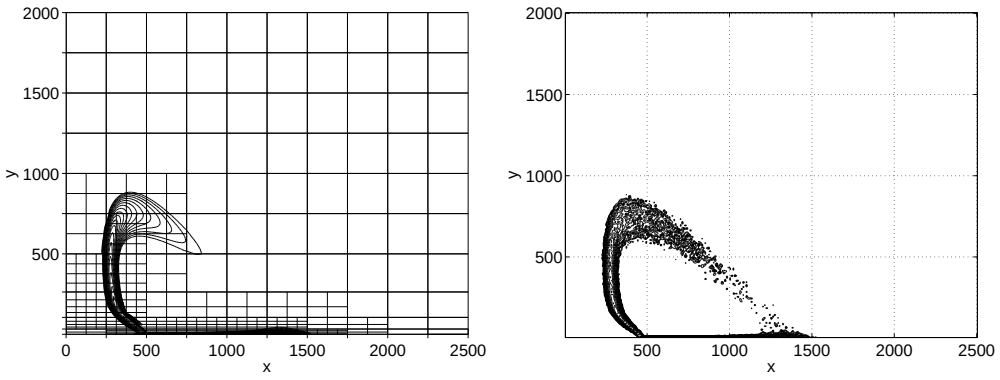

(a) (b)

Figure 8: The stationary solution computed as an eigenvector $\mathbf{p}_3^\infty$ of the zero eigenvalue (a) and the MC solution with $M = 10^5$ at $t = 1300$ (b).

The maximum of the residual $|A\mathbf{p}|_\infty$ in each period decreases by one decade in about 10^5 time steps or 300 time units in the FP solution. Hence, circa $4.4 \cdot 10^5$ steps are required for $|A\mathbf{p}|_\infty$ to converge to 10^{-4} at about $t = 1300$ when $\mathbf{p}^n$ approximates the steady state $\mathbf{p}^\infty$. The faster alternative to time integration for the steady state is to compute the eigenvector with the smallest eigenvalue as in Sect. 6.1. Three grids are generated successively with error tolerance $\epsilon_S = 0.01$ and the zero eigenvector $\mathbf{p}_3^\infty$ is computed with *eigs* requiring solutions of 60 systems of linear equations, see Fig. 8. The solution is compared to the solution with the stochastic method after more than 10^6 time steps for 10^5 trajectories. There seems to be only stochastic variation and no oscillatory variation left in $|\mathbf{p}|_\infty$ of the MC method around $t = 1300$.

The largest difference $|\delta\mathbf{p}|_\infty$ between the last time-dependent FP solution in Fig. 6 and $\mathbf{p}_3^\infty$ in Fig. 8 is 0.144. The amplitude of the oscillations in Fig. 6 is between 3.1 and 3.7 for $t > 350$ and $|\mathbf{p}_3^\infty|_\infty = 3.35$. The average of the amplitude in the MC solution at the end of the interval in Fig. 6 is 2.5 and equal to the average of $|\mathbf{p}|_\infty$ around $t = 1300$ and $t = 2000$. The difference $\delta\mathbf{p} = \mathbf{p}(1300) - \mathbf{p}(2000)$ is measured in the ℓ_1-norm over the boxes

$$\|\delta\mathbf{p}\|_1 = \sum_{i,j} |B_{ij}||\delta p_{ij}|, \tag{36}$$

where $|B_{ij}|$ is the area of B_{ij}. With a scaling such that $\|\mathbf{p}\|_1 = 1$, $\|\delta\mathbf{p}\|_1$ is 0.18 mainly due to statistical errors.

The total number of grid cells vary periodically in Fig. 9 for the FP solution. Changes of the grid occur relatively seldom at 3.7 per cent of the time steps before $t = 260$ although the impression may be different in the figure. After $t \approx 260$, the grid remains fixed. The time step is about $3 \cdot 10^{-3}$ in the whole time interval and is limited by the CFL-constraint most of the time. The average time between the events in the MC method is about 10^{-3}.

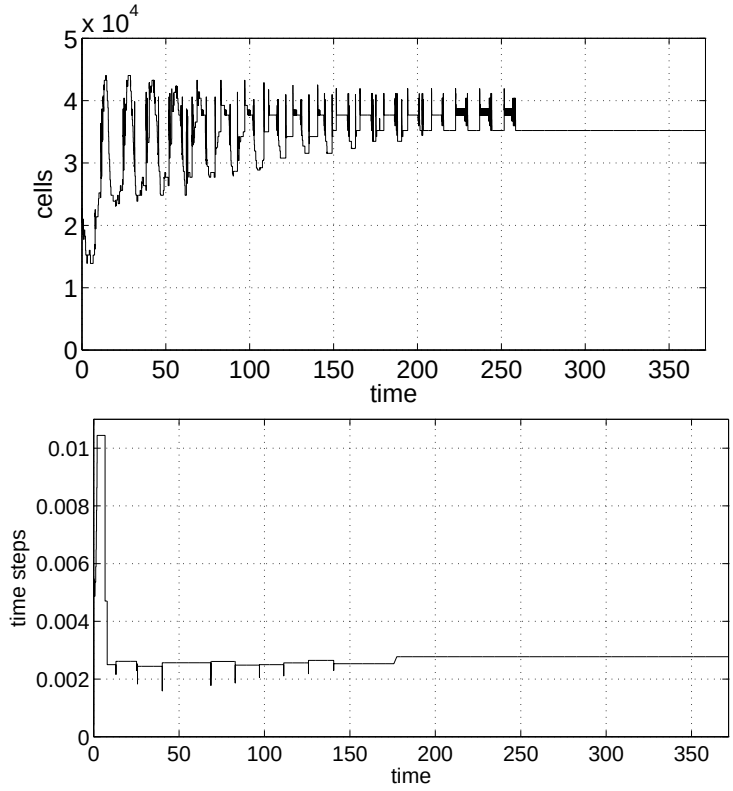

Figure 9: Time series of the number of cells (upper) and the time steps (lower).

The dependence of the MC solution on the number of trajectories is apparent in Fig. 10. The data are plotted for four different M. As expected, the smoothest isolines are obtained for the largest M.

The solutions appear to agree very well in Fig. 7. To measure the difference, every integer point in Ω is first given a probability value by the FP solution. Then let δp_{ij} be the difference between the average of the FP solution and the MC solution in the box B_{ij} and measure it in the ℓ_1-norm (36). The difference for $M = 10^3, 10^4, 10^5, 10^6$, in one period in the same time interval as in Fig. 7 is presented in Fig. 11. The solution converges almost with the expected rate $\mathcal{O}(1/\sqrt{M})$ to a solution which is slightly separated from the FP solution. Part of the explanation to this deviation is the difference between the master equation (5) approximated by the MC solution and the FP equation (6) and a small difference in the phase (see Fig. 6).

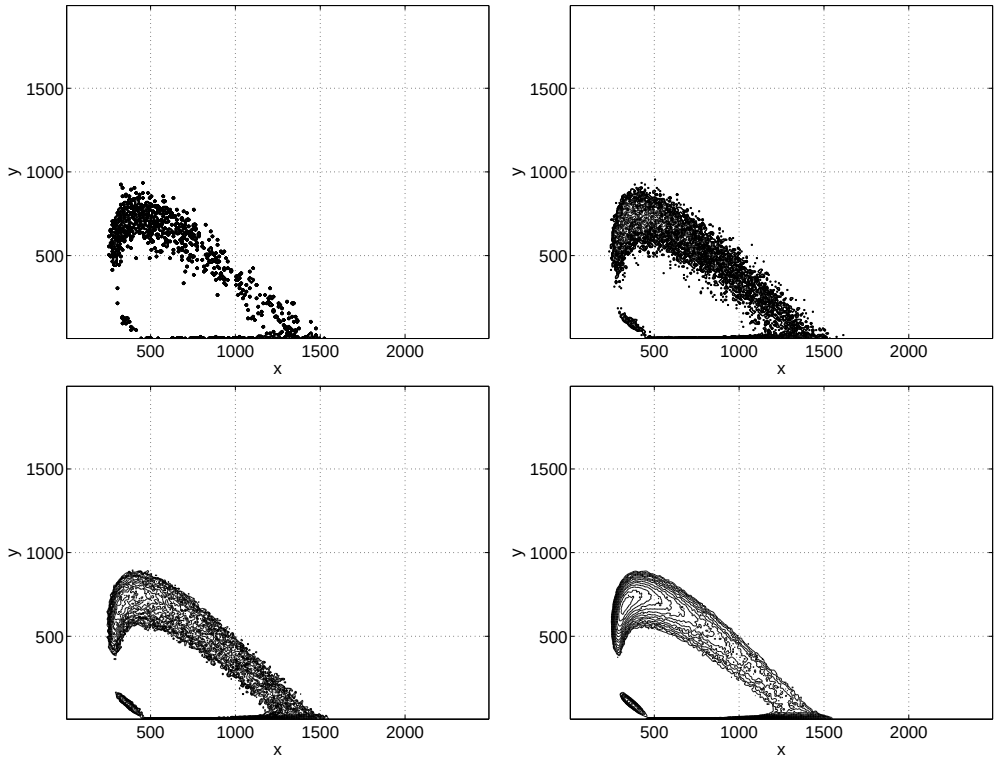

Figure 10: The isolines of the MC solution in a logarithmic scale at $t = 29.30$ for $M = 10^3, 10^4, 10^5, 10^6$, in the $(1,1), (1,2), (2,1)$, and $(2,2)$ positions in the panel matrix.

7 Conclusions

The FP equation on conservation form is discretized by a finite volume method in space and advanced in time by the BDF method of second order. The advantages of the conservation form are: The time integration is stable in the experiments, the boundary conditions are easily implemented, and the steady state solution is the eigenvector with zero eigenvalue.

The time dependent solution is computed by a method with space-time adaptivity based on estimates of the local discretization errors. The steady state solution is determined adaptively by calculating the eigenvector corresponding to the zero eigenvalue. Compared to time integration to the stationary solution, eigenvector computation with Arnoldi's method is orders of magnitude faster.

The solution of the circadian rhythm model is compared with the solution by the Gillespie algorithm. The advantages of solving the FP equation are: The solutions are smooth, the solution is computed with full error control, and there is a fast method to arrive at the steady state solution. The disadvantage is that it is directly applicable only to problems with few molecular species.

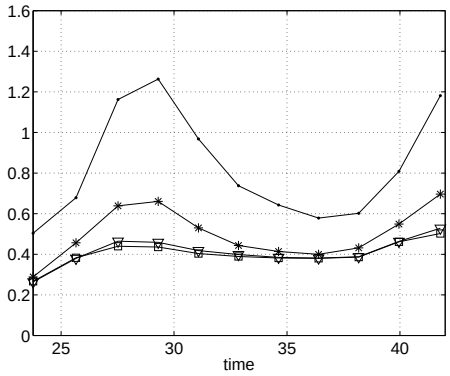

Figure 11: The difference in the solution between the FP solution and the MC solution for different number of trajectories $M : \cdot\ 10^3, *\ 10^4, \triangledown\ 10^5, \square\ 10^6$.

Acknowledgment

Many discussions with Måns Ehrenberg and Johan Elf have influenced the biological contents of this paper.

References

[1] N. Barkai, S. Leibler, Circadian clocks limited by noise, *Nature*, 403 (2000), p. 267–268.

[2] M. Berger, P. Colella, Local adaptive mesh refinement for shock hydrodynamics, *J. Comput. Phys.*, 82 (1989), p. 64–84.

[3] H.-J. Bungartz, M. Griebel, Sparse grids, *Acta Numerica*, 2004, p. 147–269.

[4] J. C. Dunlap, Molecular bases for circadian clocks, *Cell*, 96 (1999), p. 271–290.

[5] M. Ehrenberg, J. Elf, E. Aurell, R. Sandberg, J. Tegnér, Systems biology is taking off, *Genome Res.*, 13 (2003), p. 2377–2380.

[6] J. Elf, P. Lötstedt, P. Sjöberg, Problems of high dimension in molecular biology, in High-dimensional problems - Numerical treatment and applications, ed. W Hackbusch, *Proceedings of the 19th GAMM-Seminar Leipzig 2003*, p. 21-30, available at `http://www.mis.mpg.de/conferences/gamm/2003/`.

[7] J. Elf, J. Paulsson, O. G. Berg, M. Ehrenberg, Near-critical phenomena in intracellular metabolite pools, *Biophys. J.*, 84 (2003), p. 154–170.

[8] L. Ferm, P. Lötstedt, Adaptive error control for steady state solutions of inviscid flow, *SIAM J. Sci. Comput.*, 23 (2002), p. 1777–1798.

[9] L. Ferm, P. Lötstedt, Accurate and stable grid interfaces for finite volume methods, *Appl. Numer. Math.*, 49 (2004), p. 207–224.

[10] D. T. Gillespie, A general method for numerically simulating the stochastic time evolution of coupled chemical reactions, *J. Comput. Phys.*, 22 (1976), p. 403–434.

[11] A. Golbeter, Computational approaches to cellular rhythms, *Nature*, 420 (2002), p. 238–245.

[12] E. Hairer, S. P. Nørsett, G. Wanner, *Solving Ordinary Differential Equations*, 2nd ed., Springer-Verlag, Berlin, 1993.

[13] N. G. van Kampen, *Stochastic Processes in Physics and Chemistry*, North-Holland, Amsterdam, 1992.

[14] R. Keppens, M. Nool, G. Tóth, J. P. Goedbloed, Adaptive mesh refinement for conservative systems: multi-dimensional efficiency evaluation, *Comput. Phys. Comm.*, 153 (2003), p. 317–339.

[15] R. B. Lehoucq, D. C. Sorensen, C. Yang, *ARPACK Users' Guide: Solution of Large-Scale Eigenvalue Problems with Implicitly Restarted Arnoldi Methods*, SIAM, Philadelphia, 1998.

[16] P. Lötstedt, S. Söderberg, A. Ramage, L. Hemmingsson-Frändén, Implicit solution of hyperbolic equations with space-time adaptivity, *BIT*, 42 (2002), p. 134-158.

[17] K. W. Morton, *Numerical Solution of Convection-Diffusion Problems*, Chapman & Hall, London, 1996.

[18] Y. Saad, M. H. Schultz, GMRES: A generalized minimal residual algorithm for solving nonsymmetric linear systems, *SIAM J. Sci. Stat. Comput.*, 7 (1986), p. 856–869.

[19] M. Thattai, A. van Oudenaarden, Intrinsic noise in gene regulatory networks, *Proc. Nat. Acad. Sci.*, 98 (2001), p. 8614–8619.

[20] J. M. G. Vilar, H. Y. Kueh, N. Barkai, S. Leibler, Mechanisms of noise-resistance in genetic oscillators, *Proc. Nat. Acad. Sci.*, 99 (2002), p. 5988–5992.